Influence of the reaction temperature on the oxygen reduction reaction on the metal-free nitrogen-doped carbon nanotubes catalysts

Lai Truong-Phuoc[a*], Cuong Duong-Viet[a,b], Won-Hui Doh[a,d], Antoine Bonnefont[c], Izabela Janowska[a], Dominique Begin[a], Elena R. Savinova[a], Pascal Granger[d], Cuong Pham-Huu[a*]

[a]*Institut de Chimie et Procédés pour l'Energie, l'Environnement et la Santé (ICPEES), ECPM, UMR 7515 du CNRS-Université de Strasbourg, 25 rue Becquerel, 67087 Strasbourg Cedex 02, France.*

[b]*Ha-Noi University of Mining and Geology, Dong Ngac Tu Liem - Ha Noi – Viet Nam.*

[c] *Laboratoire d'Electrochimie et de Chimie Physique du Corps Solide, Institut de Chimie de Strasbourg (ICS) - UMR 7177 du CNRS - Université de Strasbourg, 4, rue Blaise Pascal, CS 90032, F - 67081 Strasbourg Cedex, France.*

[d]*Unité de Catalyse et Chimie du Solide (UCCS), UMR 8181 du CNRS-Université de Lille-1, Bâtiment C3, Université Lille 1, 59655 - Villeneuve d'Ascq Cedex, France.*

Corresponding author: cuong.pham-huu@unistra.fr (C. Pham-Huu), truongphuoc@unistra.fr (L. Truong-Phuoc)

Abstract

Keywords:

Catalysis – Nitrogen-doped carbon nanotubes – Oxygen reduction reaction - Electrocatalysis

Metal-free nitrogen-doped carbon nanotube (N-CNT) catalysts were synthesised via chemical vapour deposition (CVD) method at 700°C and were used as metal-free catalyst in the oxygen reduction reaction. The activity and stability of these N-CNTs were studied as a function of the reaction temperature. The kinetic analysis of these catalysts was also carried out and compared to the ORR performance of the commercial catalyst Pt/C Vulcan XC72. N-CNT700BW, without any chemical treatment after the CVD synthesis, catalyst possess an $E_{1/2}$ at 50mV lower and a J_k at 0.9V 10 times less than Pt/C. The activation energy of the N-CNT-based catalysts was calculated and is around 70 kJ. mol^{-1}. A long-term stability test has also been conducted and shows the high stability of the N-CNT-based catalysts compared to that of the Pt-based catalyst where a significant loss of ORR activity was observed after 1,500 cycles.

1. Introduction

The oxygen reduction reaction (ORR) is of critical importance to support industrial development of fuel cells and metal-air batteries for the future energy mix infrastructure (1-3). The main drawback of the ORR is its extremely low rate compared to that of the anode hydrogen oxidation which severely limits the application of fuel cells. To date, platinum-based catalysts are the most active ones for such reaction, however, it suffers from high cost, low tolerance to poisons such as methanol and CO, and low stability (4). A large number of investigations have been devoted to the replacement of platinum by other catalysts including Pt-based alloys (5, 6), transition metal (7) and carbon-based materials doped with various elements (8).

Nitrogen-doped carbon composites such as nitrogen-doped carbon nanotubes/nanofibers and/or mesoporous carbon have received a growing academic and industrial interest, as metal-free catalysts, in several catalytic applications during the last decades [9-14]. These composites, either in a bulk or supported forms, are mostly synthesized via chemical vapor deposition (CVD) process using different sources of carbon and nitrogen precursors and iron as growth catalyst [15-21]. Beside its use as catalyst support in several reactions nitrogen-doped carbon nanotubes (N-CNTs) is also extensively employed as metal-free catalyst for replacing platinum in the cathode oxygen reduction reaction (ORR) for fuel cells application [22-26].

In general, the ORR is operating at temperature close to the maximum affordable temperature of the Nafion® which is close to 80 °C. It is expected that such reaction temperature could increase the corrosion of the metal to a certain extend which directly influence the ORR performance as a function of time of operation. It is of interest to be able to correlate the stability of the metal-free N-doped carbon catalysts with that of the Pt/C, not only at room temperature, but also at higher operating temperature. He et al. (27) and Zhang et al. (28) have recently reported a large deactivation of the Pt/C catalyst as a function of cycling tests at room

temperature. Such deactivation could be attributed to the metal leaching from the catalyst surface over time by reaction with the acid or alkaline media. On the other hand, one should expect a higher stability for the N-CNTs due to the fact that the nitrogen atoms are directly included in the carbon lattice which provides higher stability towards leaching and also strengthen the chemical inertness character of the material.

Herein, we report on the stability of the metal-free N-CNTs catalysts as a function of the reaction temperature (25 to 75°C) on a Rotating-Ring Disk Electrode (RRDE), supplied from Pine Instruments, and cycling tests in the ORR experiments. The results will be also compared with those obtained on a reference 20 wt.% Pt/C catalyst. It is expected that such investigation will be of extreme interest for the future development of these metal-free catalysts in the field of fuel cell application where long-terms stability is a prerequisite.

2. Experimental

2.1 N-CNTs synthesis

The N-CNT was synthesized according to the Chemical Vapor Deposition (CVD) method with iron supported on alumina as growth catalyst [29]. Fe (20 wt %)/Al_2O_3 catalyst was synthesized by impregnating γ-Al_2O_3 support (… m^2/g) with an aqueous solution containing $Fe(NO_3)_3$. The theoretical iron loading was fixed at 20 wt %. The solid was dried at room temperature overnight and oven-dried at 110 °C for 24 h. It was then calcined in air at 350 °C for 2 h in order to decompose the nitrate precursor into its corresponding oxide. The Fe_2O_3/Al_2O_3 catalyst was housed in a quartz reactor localized inside an electric furnace. The catalyst was reduced under hydrogen flow (200 mL/min) at 400 °C for 2 h and then, the reaction temperature was raised to the synthesis temperature (heating rate of 10 °C/min) and the H_2 flow was replaced by a $C_2H_6/NH_3/H_2$ (x/y/z mL/min) mixture. XRD analysis of the iron-based

growth catalyst after calcination and reduction (not shown) confirms the complete reduction of Fe_2O_3 to metallic Fe^0. The C_2H_6, NH_3, and H_2 flow rates, used in the synthesis of N-CNT, were fixed at 50:50:20 sccm. min^{-1}. The synthesis was lasted for 2 h, and the reactor was cooled to room temperature under argon and we obtained the as-synthesized N-CNT700BW catalyst. Then this product was treated by a NaOH (20 wt. %) solution at 80 °C for 24 h followed by an acid treatment (HNO_3, 32 vol. % at 80 °C) for 24 h in order to remove both the support and the growth catalyst. The obtained N-CNT700AW was washed thoroughly with distilled water between the treatment processes. Elemental analysis performed on the treated N-CNTs indicates that ~1.5 at.% of residual iron remains in the N-CNT700BW catalyst and ~0.12 at.% in the N-CNT700AW. Such residual iron could be attributed to the iron encapsulated within the carbon nanotubes which was not accessible to the acid during the purification process.

2.2 ORR experimental setup

Electrochemical studies were performed at 25 - 75°C in a three-electrode cell in 0.1 M KOH supporting electrolyte, using Autolab PGSTAT30 (Eco Chemie, The Netherlands) potentiostat equipped with an analogue linear sweep generator at the sweep rate of 10 mV s^{-1}. Mercury oxide (Hg/HgO) electrode and Pt-wire electrodes were used as reference and counter electrodes, respectively. Unless otherwise stated, all potentials hereinafter are referred to the reversible hydrogen electrode (RHE).

For the ink preparation, 10.0 mg of the catalyst sample, 5 mL isopropanol, and 50µL Nafion solution (5 wt %) were ultrasonically mixed to form a homogenous catalyst ink. For the RRDE test, the working electrode (PINE, AFE6R2GCPT) was prepared by loading 52.5 µL of catalyst ink onto a pretreated glassy carbon (GC) electrode (5.5 mm diameter and 0.2376 cm^2 geometrical area) and then dried at room temperature. The reference Pt/C catalyst was recorded

with a 20 wt.% Pt/C (Sigma) catalyst at a loading of 125 $\mu g_{Pt/C}$ cm^{-2}. The N-CNT loading was set at 445 $\mu g_{N\text{-}CNT}$ cm^{-2} for both untreated and treated ones.

All aqueous solutions were prepared using ultrapure water (18MΩcm, < 3 ppb TOC) and supra-pure KOH (Sigma-Aldrich). O_2 was constantly bubbled through the solution during O_2-reduction experiments in order to maintain the saturation level and the ring potential was set at 1.2 V RHE in accordance with previous studies. Collection efficiency (N) was calculated from the experimental data obtained in 10 mM K_3FeCN_6 in 0.1M NaOH at standard measurement conditions (potential sweep rate 10 mV. s^{-1}, 25°C). The collection efficiency for the Pt (20%)/C Vulcan electrode was found to be 37%, this value is also reported by Chlistunoff [30].

The four-electron selectivity of catalysts was evaluated based on the H_2O_2 yield, calculated from the following Eq. (1)

$$H_2O_2\,(\%) = 200(J_R/N)/(J_R/N\text{-}J_D) \qquad (1),$$

where J_D and J_R were the disk and ring currents density, respectively, and *N* the ring collection efficiency.

The electron transfer number can be calculated in two ways. The first is to use the ring current and the disk current $n = -4J_D/(J_R/N\text{-}J_D)$. The second way to calculate n is by using the first-order Koutecky-Levich equation (see Eq. (2)):

$$1/J_D = 1/j_k + 1/j_d$$

where j_k was the kinetic current density and j_d the diffusion-limited current density through the expression $j_d = B\omega^{1/2} = 0.62nF\gamma^{-1/6}D_{O2}{}^{2/3}C_{O2}\omega^{1/2}$. n was the average electron transfer number, *F* is the Faraday constant, γ is the kinematic viscosity of the electrolyte; D_{O2} the oxygen diffusion coefficient (1.15×10^{-5} $cm^2.s^{-1}$ C_{O2} the bulk oxygen concentration in the electrolyte (1.4×10^{-6} $mol.cm^{-3}$) and ω the angular velocity of the electrode. The kinetic current density (j_k) and the Koutecky-Levich slope ($1/B$) can be obtained from a plot of $1/j$ versus $\omega^{-1/2}$.

3. Results and discussion

3.1 Characteristics of the N-CNTs

The representative SEM and TEM micrographs of the N-CNTs synthesized at 700 °C are presented in Fig. 1. SEM micrographs show a relatively high homogeneous diameter of the as-synthesized N-CNTs which is centered at around 80 nm and length up to several tenth micrometers (Fig. 1A and B). The N-CNTs are highly entangled from each other forming bundles according to the SEM analysis. TEM micrograph of the as-synthesized sample (Fig. 1C) shows the bamboo-like microstructure of the sample with remote compartments along the tube axis according to the recent TEM tomography analysis (31). High resolution TEM micrograph (Fig. 1D) also evidences the high graphitization of the tube wall and the complete absence of carbon nanoparticles which confirm the high selectivity of the CVD synthesis method (32-36). TEM analysis of the sample after acid treatment do not reveal modification compared to that after synthesis (Fig. 1E and F). It is expected that for the relatively mild acid/base treatment used in the present work the microstructure of the sample was not altered and only the chemical surface and nitrogen content were modified (see below).

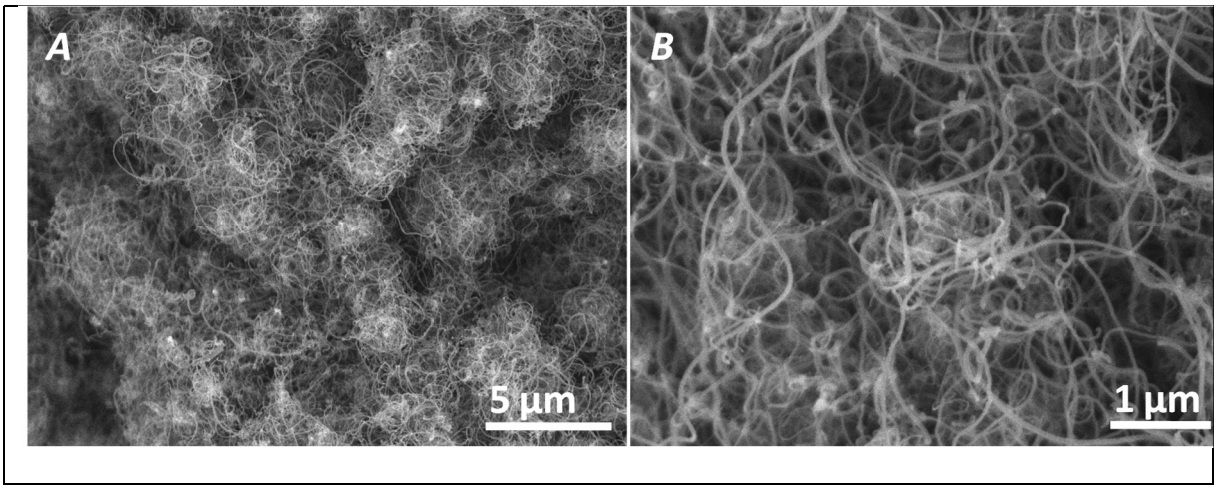

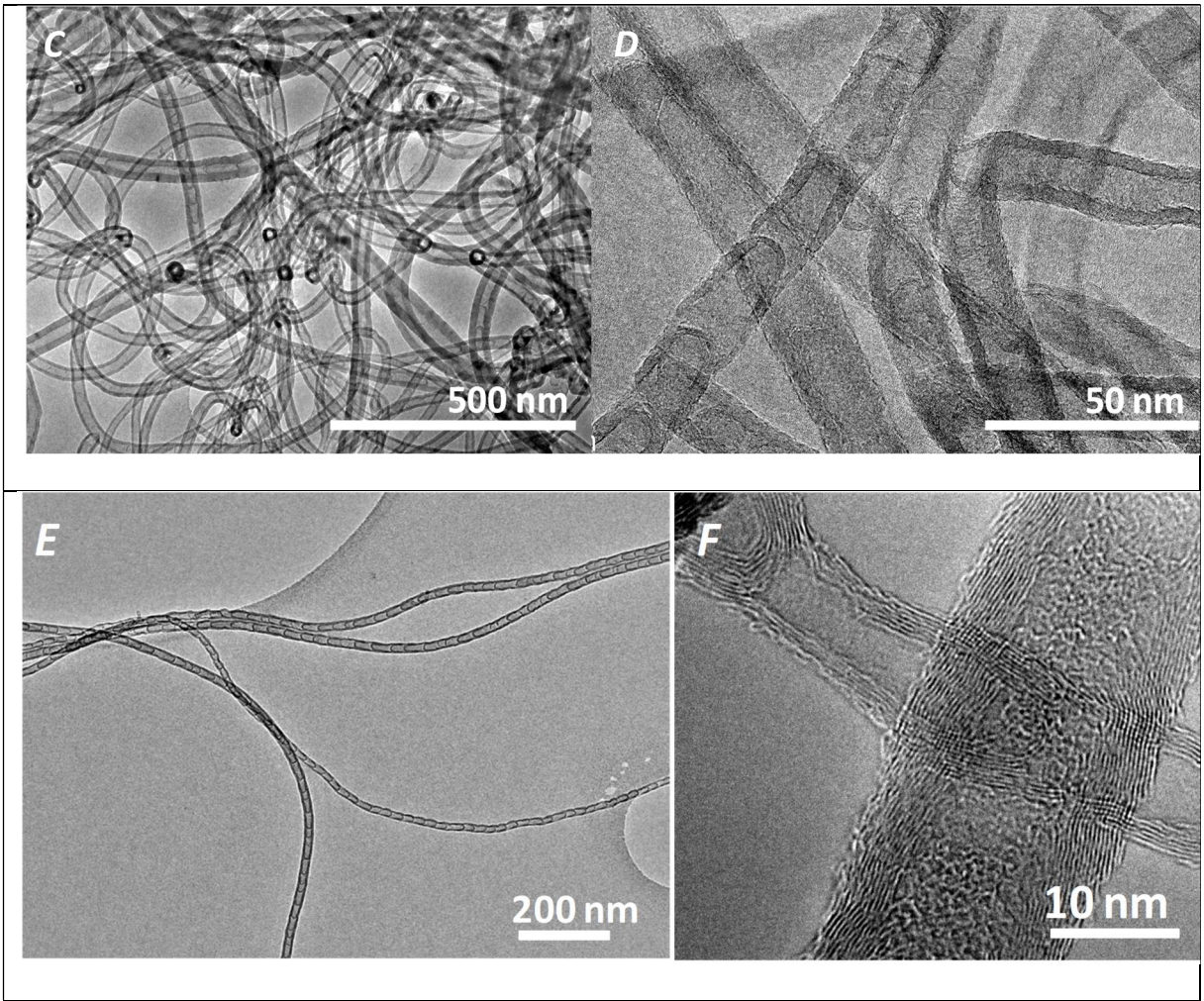

Fig. 1. (A, B) SEM and (C-D) TEM micrographs of the N-CNTs synthesized at 700 °C under a mixture of $C_2H_6/H_2/NH_3$ without any chemical treatment and (E-F) after acid treatment showing the preservation of the material microstructure.

The specific surface area of the N-CNTs, measured by N_2 adsorption at -196 °C, was around 200 $m^2.g^{-1}$, which is close to the current values reported for such material in the literature (32-36). However, it is worthy to note that such surface area is only accounted to the outer surface of the material as the N-CNTs are constituted by a bamboo-like structure with remote compartment which hinders the access of both gaseous and liquid reactants to the inner surface of the tube. Such compartmented structure also hinders the full exposure of the nitrogen sites

in the catalyst for the ORR reactants. Work is ongoing using ball-milling technique to break down the tube wall in order to increase the density of nitrogen sites for the reaction of interest.

The nature of the different nitrogen species in the sample, before and after acid washing, is analyzed by mean of the X-ray photoelectron spectroscopy (XPS) and the results are presented in Fig. 2A. The XPS N1s spectrum reveals after decomposition the presence of four types of nitrogen species, i.e. pyridinic (N_P), pyrrolic (N_{PY}), quaternary (N_Q) and incorporated (N_I), in good agreement with the literature reports (37-39). The total nitrogen doping and the percent of the different nitrogen species are presented in Table 1. According to the XPS data one can see that the chemical treatment, i.e. basic and acidic washing, leads to a significant decrease of the total nitrogen content in the catalyst along with the decrease of the N_P and N_I and an increase of the N_{Py} and N_Q (the change on this later is less pronounced). These results indicate that chemical treatment alters the nitrogen surface functionalities of the catalyst.

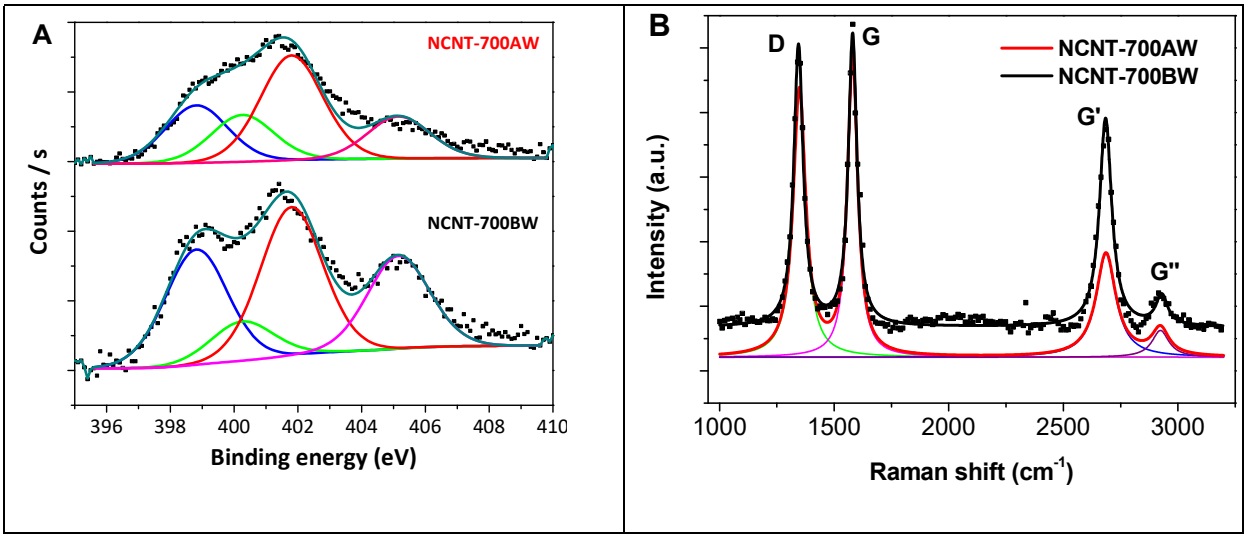

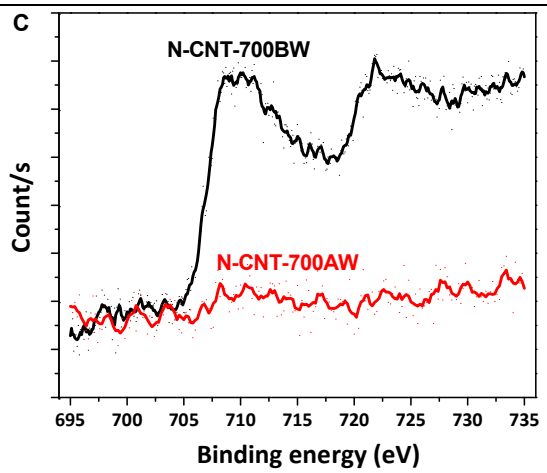

Fig. 2. (A) XPS N1s and (B) Raman spectra of the N-CNTs synthesized at 700 °C, before (BW) and after (AW) washing with acid solution. (C) Corresponding XPS Fe 2p spectra of the samples before and after acid treatment showing a quasicomplete removal of the residual iron species at the surface.

The Fe 2p XPS spectra of the N-CNT before and after washing catalysts are shown in Fig. 2.C. In the untreated sample, i.e. N-CNT-700BW, the residual iron species contributes to about 0.4 at %. The atomic percentage of iron in N-CNT-700AW is very low, and confirms the quasi-complete removal of the iron growth catalyst after the acidic treatment. In addition, the remaining iron species are mostly encapsulated within the graphene layers and thus, are no longer accessible for the reaction.

Table 1. The chemical composition of the N-CNT-based catalysts determined by XPS and elemental analysis performed on the chemical treated sample.

	C	O	Fe	N	N_P	N_{Py}	N_Q	N_I
N-CNT700BW	88.4	5.3	1.5	4.3	29.1	9.8	37.5	23.5
N-CNT700AW	90.6	7.1	0.06	2.2	22.8	18.8	41.5	17.0

Elementary analysis of the N-CNT700AW	90.7	7.4	0.08	1.9	-	-	-	-

The graphitization degree of the N-CNT-700 sample was also analyzed by Raman spectroscopy. The Raman spectra were fitted to Lorentz-shaped components (Fig. 2.B) and showed two intense first order Raman lines at 1340 cm^{-1} (D-band) and 1580 cm^{-1} (G-band) and two other second order features at 2690 cm^{-1} (G'-band) and 2920 cm^{-1} (a combination of the D and G bands) (40). The ratio of D to G band intensities I_D/I_G is identical for both of N-CNT-based catalysts (around 0.9) that mean they present the same degree of crystalline. But the higher intensity of the G' band of N-CNT-700BW confirm the higher nitrogen content in this sample than in the same after chemical treatment, N-CNT-700AW, which is also consistent with the XPS results reported above.

3.2 ORR performance as a function of the reaction temperature

The ORR activity, as a function of the reaction temperature, measured on the different catalysts is presented in Fig. 3.

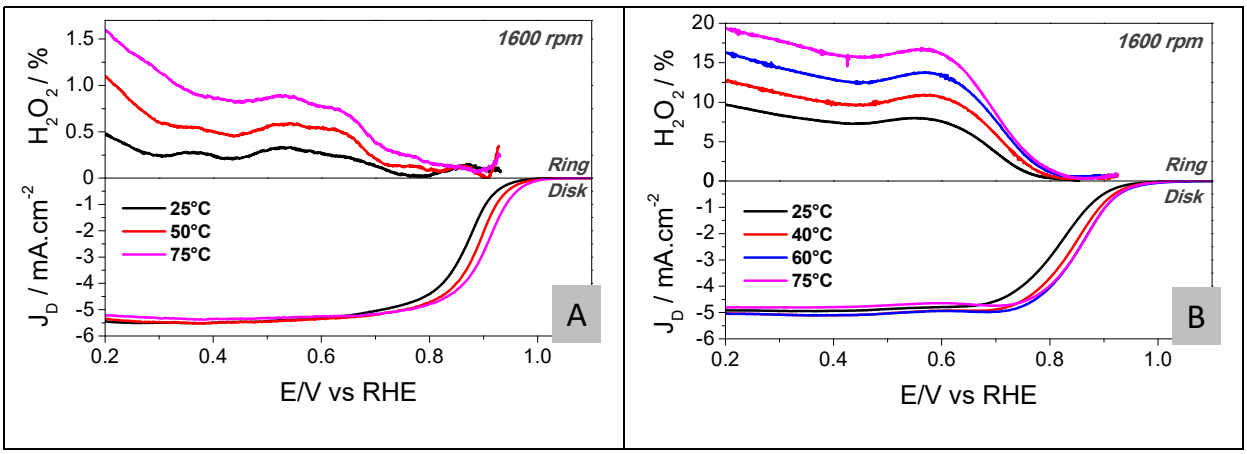

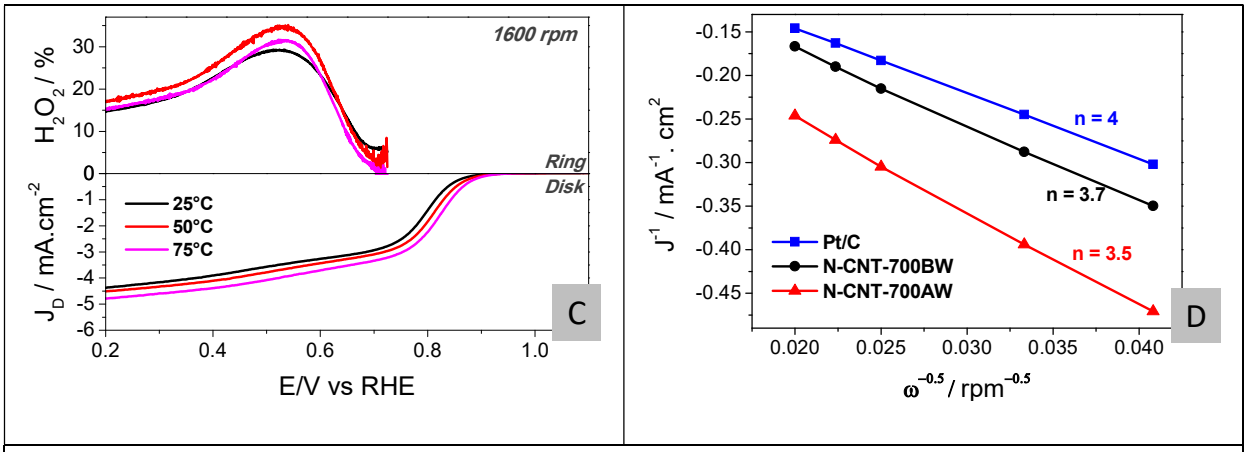

Figure 3. ORR performance as a function of the testing temperature on the different catalysts. (A) Pt/C, (B) N-CNT-700BW, (C) N-CNT-700AW. (D) K-L slope at 0.4V showing the average number of transfer electrons on the different catalysts.

On the different catalysts, a rise in reaction temperature leads to an increase of the $E_{1/2}$ value (Table 3) whereas a higher H_2O_2 concentration was observed, i.e. 1.6 % at 75 °C instead of 0.5 % at 25 °C for Pt/C and 20% at 75°C instead of 10% at 25°C for the N-CNT-700BW catalyst. Therefore, the mean transferred electron number from 0.2V to 0.7V (diffusion plateau) calculated by RRDE method decrease as a function of the reaction temperature. It is worthy to note that the mean electron number decreases in a lesser extend for Pt/C and N-CNT700AW catalysts while significant decrease was observed for the N-CNT700BW catalyst. Such observation could be explained by the increase of desorption rate of H_2O_2 at higher testing temperature in particular with the presence of iron residual in N-CNT700BW. Additional work is underway to get more insight about such phenomenon. Figure 3D showed the Koutecky-Levich (K-L) slope calculated at E = 0.4V and 25°C for the different tested catalysts. This slope leads to thecalculation of the electron transfer numbers respectively equal to 4, 3.7 and 3.5 for Pt/C, N-CNT-700BW and N-CNT-700AW catalysts. Hence, N-CNT-based catalysts present a

mechanism close to $4e^-$ pathway but the $2e^-$ pathway mechanism seems unavoidable due to the presence of prismatic sites or structural defaults of carbon nanotubes.

Table 3. $E_{1/2}$ and the average electron transfer on the different catalysts as a function of the reaction temperature.

	T°C	$E_{1/2}$ /mV	n (K-L plot at 0.4V) / e-	n (RRDE) / e-
Pt/C	25	865	4	3.994
	75	905	-	3.980
N-CNT-700BW	25	815	3.7	3.84
	75	860	-	3.67
N-CNT-700AW	25	770	3.5	3.58
	75	795	-	3.51

Fig. 4 illustrates the variation of average electron transfer number (*n*) as a function of the ORR reaction temperature. As observed, n decreases with temperature for all catalysts in particular on N-CNT-700BW which contains more residual iron species.

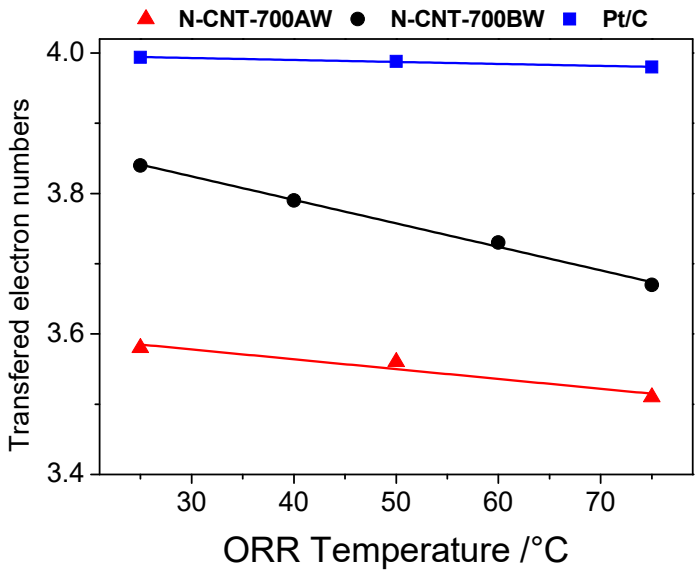

Figure 4. Variation of the average electron transfer number (*n*), calculated from 0.2 to 0.7V by RRDE method, as a function of the ORR reaction temperature

Fig. 5 shows the Tafel plots for the mass transfer corrected to the mass-specific current densities at 25°C and 75°C for O_2 reduction on N-CNT-700BW and Pt/C catalysts, obtained from the positive-going sweep direction at 2500 rpm. We calculated the experimental data to the two Tafel slope regions at low (> 850 mV) and high (< 800mV) overpotentials. The resulting Tafel slopes are given in Table 3. They are in good agreement with literature data and are centred at around -2.3RT/F ~ 60 mV. dec^{-1} at low over-potentials and around -2 x 2.3RT/F ~ 120 mV. dec^{-1} at high over-potentials. The Tafel slopes around 70 mV. dec^{-1} of N-CNT-700BW showed that this catalyst is slightly less active than Pt/C. This value is comparable with the results of Wong et al. (41) which was around 75 - 84 mV. dec^{-1}.

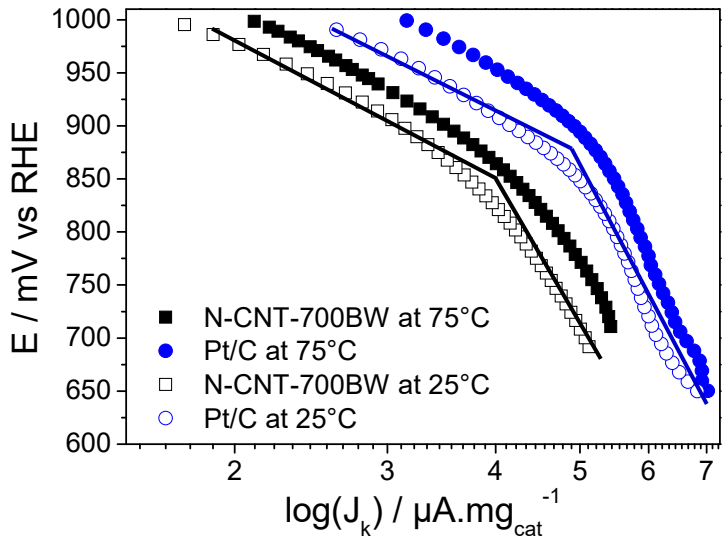

Figure 5. Mass transport corrected mass-specific current densities for the ORR on N-CNT-700BW (black) and Pt/C (blue) at 25 and 75°C in 0.1M KOH, saturated with pure O_2 at 1 bar.

Table 3. Low- and high-current density Tafel slopes (TS) for the ORR on N-CNT-700BW and Pt/C in 0.1M KOH, saturated with pure O_2 at 1 bar.

	TS/mV.dec^{-1} for E > 850 mV	TS/mV.dec^{-1} for E < 850 mV
N-CNT-700BW, 25°C	73	120
N-CNT-700BW, 75°C	70	121
Pt/C, 25°C	59	122
Pt/C, 75°C	65	120

In order to compare the activity of different catalysts, the kinetically controlled current density at a potential of 900 mV, corresponding to negligible mass transport phenomena, are calculated according to the expression $J_k = J*J_L/(J_L-J)$. The results obtained on Pt/C and N-CNT700BW at 25 and 75°C are compared in Table 4. One can see that the activity of N-

CNT700BW catalyst is about 10 times lower than that of Pt/C at 25°C and about 25 times lower at 75°C. According to the results we can state that the ORR activity of the N-CNT based catalyst is much lower than the one obtained on the Pt/C catalyst under similar reaction conditions. It is also worthy to note that in the N-CNT-based catalysts the nitrogen atoms are randomly distributed within the solid matrix and, due to the closed morphology of the bamboo-like structure, most of the nitrogen sites is not accessible to oxygen molecules for the reaction as discussed above.

Table 4. Catalytic current comparison for the ORR on N-CNT-700BW and Pt/C in 0.1M KOH, saturated with pure O_2 at 1 bar.

	T°C	J_k at 0.9V / $mA.mg_{active\ phase}^{-1}$
Pt/C	25	14.8
Pt/C	75	83.6
N-CNT700BW	25	1.3
N-CNT700BW	75	3.3

The activation enthalpies (ΔH^*) for the ORR are evaluated at fixed over-potentials using the Arrhenius equation $\Delta H^* = d(\ln J_k)/d(1/RT)$ (42). The Arrhenius plots at an over-potential η = 350 mV are showed in Fig. 6 for both Pt/C and N-CNT700BW catalyst. The activation enthalpies determined are 57 and 70 $kJ.mol^{-1}$ respectively. Similar activation enthalpie of ~ 58 $kJ.mol^{-1}$ were observed by Beattie et al. (44) for Pt/C in 0.5M H_2SO_4 (43). Jiang et al. also calculated this parameter in alkaline medium and gave a value of 48 $kJ.mol^{-1}$ at an over-potential of 300 mV. Moreover, Markovic et al. reported that the ORR activation energy of Pt single crystal of approximately 45 ± 5 $kJ.mol^{-1}$ is pH independent and structure insensitive

(45). This result indicates that it is of interest to design a higher temperature alkaline fuel cell for N-CNT catalyst.

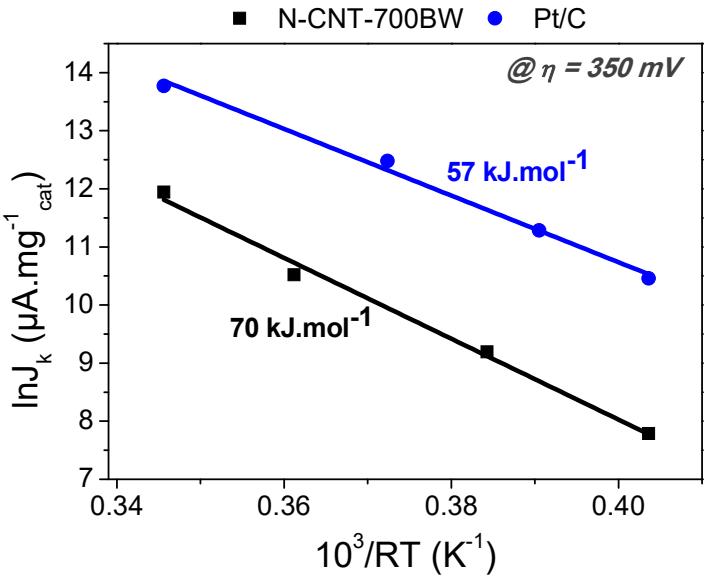

Figure 6. Arrhenius plots for the mass-specific current densities for the ORR at an over-potential of 350 mV for the on Pt/C (blue) and N-CNT-700BW (black).

3.3 ORR stability as a function of cycling tests

The ORR stability on the different catalysts as a function of cycling tests at 75°C is presented in Figs. 7.A- C. On the Pt/C catalyst a sharp deactivation is observed up to 750 cycles and becomes slower after. The N-CNT-based catalysts show much lower deactivation as a function of cycling tests unlikely to what was observed on the Pt/C catalyst operated under similar reaction conditions.

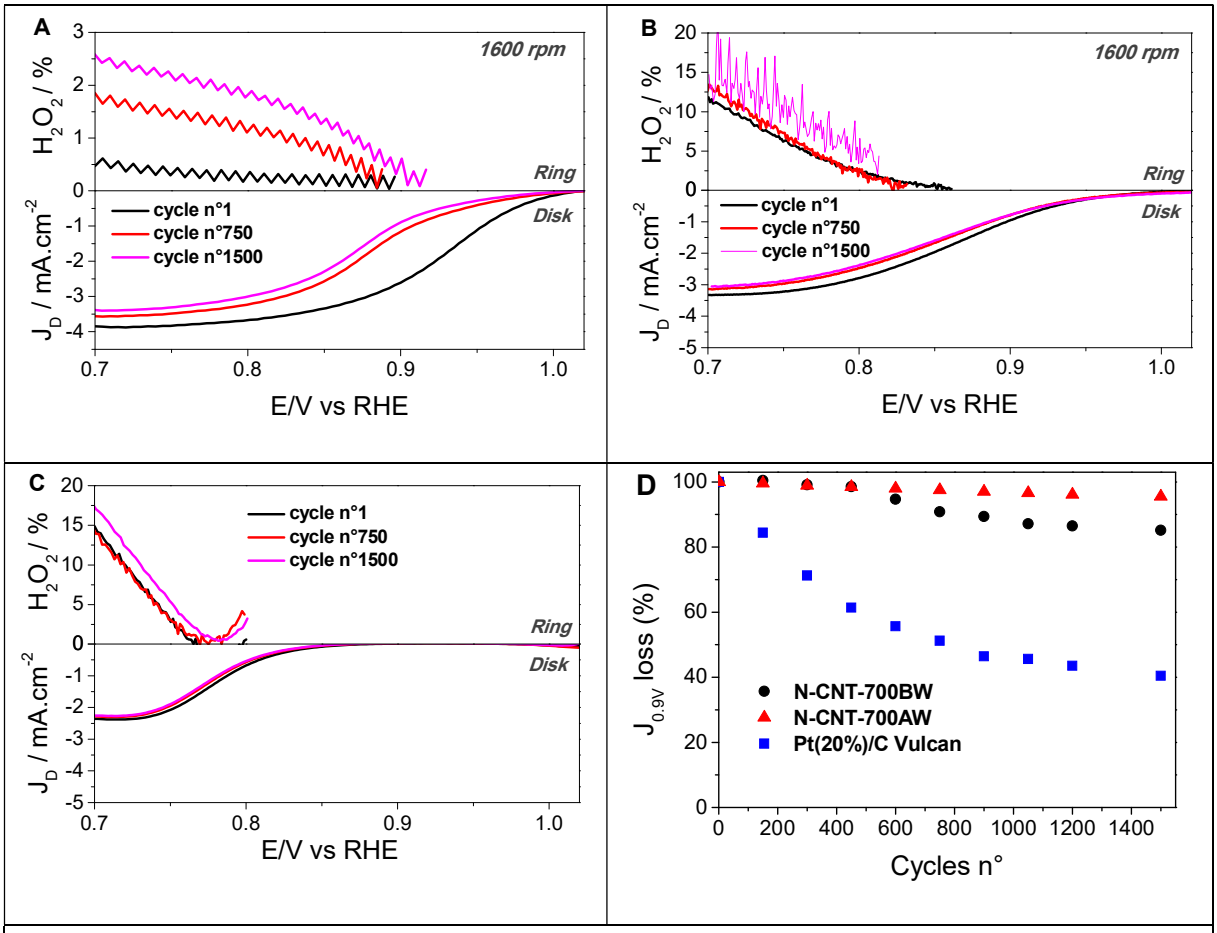

Figure 7. ORR stability as a function of the cycling tests at 75 °C on the different catalysts. (A) Pt/C, (B) N-CNT-700BW, (C) N-CNT-700AW and (D) $J_{0.9V}$ loss after 1500 cycles.

The ORR performance of the different tested catalysts recorded at $J_{0.9\ V}$ and at 75 °C, with continuous potential cycling between 1V and 0.7V in O_2-saturated 0.1 mol. L^{-1} KOH, is presented in Fig. 7 as a function of the number of cycling tests. According to the results, Pt/C exhibits a drastic deactivation up to 1,000 cycles corresponding to 50 % loss of the the initial ORR activity. The deactivation observed on the Pt/C catalyst could be attributed to the sintering of the metal nanoparticles or to the surface modification of the carbon support during the cycling tests. On the other hand, on both the N-CNT-based catalysts, either washed with acid or not, display a net lower deactivation behavior as a function of the cycling tests under similar reaction

conditions. Among them, the acid treated sample (N-CNT-700AW) is the less affected one with only less than 5 % activity lost after 1,500 cycles. Similar results have already been reported by He et al. (27) during the ORR cycling tests on the nitrogen-doped graphene catalyst. The slightly higher deactivation rate observed on the unwashed sample (N-CNT-700BW) could be attributed to the leaching of the residual iron metal over time. However, it is worthy to note that the ORR activity of the Pt/C catalyst, even after drastic deactivation as a function of the cycling tests, is still the most active among the tested catalysts under the operated ORR experiments.

4. Conclusion

The results obtained have clearly evidence the high sensibility of the Pt/C catalyst towards deactivation as a function of the cycling tests. In addition, the stability of the Pt/C catalyst is also extremely sensitive towards the reaction temperature, i.e. more pronounced deactivation as increasing the ORR testing temperature. Such results could be attributed to the corrosion effect during the cycling tests which remove part of the noble metal catalyst and also the carbon support which leads to a significantly decrease of the density of active sites for the reaction.

The high stability of the N-CNTs catalysts, after acidic treatment, could be attributed to the lack of corrosion process induced by the alkaline medium to the catalyst unlikely to that was occurred with both the Pt/C and unwashed N-CNT where some residual iron species with ORR activity could be present. In the N-doped carbon catalysts the ultra-stable nitrogen-site which was generated by the replacement of the nitrogen atom in the carbon lattice seems to be much less affected by the reaction medium. Such result is of extreme interest in regard to the development of a noble metal-free and long-life stable catalyst for the ORR process.

The ORR activity of the Pt/C catalyst is significantly higher than that of the N-CNT catalysts under similar reaction conditions. The ORR activity of the N-CNT can be improved

by increasing the catalyst amount per surface of the electrode. However, such modification also induces problems of diffusion and resistance throughout the electrode thickness, especially for the MEAs testing setup. Work is ongoing to improve the intrinsic ORR activity of the N-CNT catalysts by modifying the amount of the doping and or chemical surface of the catalyst and also to evaluate the ORR performance of these N-CNT catalysts in another reaction namely direct methanol alkaline fuel cell where a higher sensitivity of platinum is reported (DMFC).

Acknowledgements

The present work is financially supported by a European project (FREECATS) under a contract number NMP3-SL-2012-280658. LTP would like to thank the EU for the grant during their postdoctoral stay at the ICPEES. DVC would like to thank the Vietnamese government for the grant during his stay at the ICPEES. Dr. W. Baaziz and T. Romero (ICPEES) are gratefully acknowledged for performing TEM and SEM analysis of the sample. The SEM and TEM experiments were carried out at the facilities of IPCMS (UMR 7504 CNRS-UdS).

References

1. R. Schlögl, “Chemical Conversion and Storage” (Ed. R. Schlögl), de Gruyter, Berlin, Boston (2013) 1-34 and references therein.
2. Winter M. and Brodd R. J., Chem. Rev. 104 (2004) 4245-4269.
3. S. Basu, Ed., Recent Trends in Fuel Cell Science and Technology, Springer, New York, 2007.
4. N. M. Marković, T. J. Schmidt, V. Stamenković and P. N. Ross, Fuel Cell 1 (2001) 105-116.
5. V. M. V. Lebedeva, V. Pierron-Bohnes, C. Goyhenex, V. Papaefthimiou, S. Zafeiratos, R. R. Nazmutdinov,V. Da Costa, M. Acosta, L. Zosiak, R. Kozubski, D. Muller, E. R. Savinova, Electrochimica Acta 108 (2013) 605-616.
6. J. Greeley, I. E. L. Stephens, A. S. Bondarenko, T. P. Johansson, H. A. Hansen, T. F. Jaramillo, J. Rossmeisl, I. Chorkendorff & J. K. Nørskov, Nature Chemistry 1 (2009) 552 – 556.
7. G. Wu, P. Zelenay, Nanostructured Nonprecious Metal Catalysts for Oxygen Reduction Reaction, Acc. Chem. Res. 46 (2013) 1878–1889
8. Wang D.-W., Su D. S., Ener. Environ. Sci. 7 (2014) 576-591.
9. C. Duong-Viet, L. Truong-Phuoc, T. Tran-Thanh, J. M. Nhut, L. Nguyen-Dinh, I. Janowska, D. Begin, C. Pham-Huu, Appl. Catal. A: Gen. 482 (2014) 397-406.
10. K. Chizari, A. Deneuve, O. Ersen, I. Florea, Y. Liu, D. Edouard, I. Janowska, D. Begin, C. Pham-Huu, ChemSusChem 5 (2012) 102-108.
11. H. Wang, T. Maiyalagan, X. Wang, ACS Catal. 2 (2012) 781-794.
12. D. S. Su, J. Zhang, B. Frank, A. Thomas, X. Wang, J. Paraknowitsch, R. Schlögl, ChemSusChem 3 (2010) 169-180.

13. S. van Dommele, K. P. de Jong, J. H. Bitter, Chem. Commun. 46 (2006) 4859-4861.
14. J. Luo, F. Peng, H. Wang, H. Yu, Catal. Commun. 39 (2013) 44-49.
15. M. Terrones, H. Terrones, N. Grobert, W. K. Hsu, Y. Q. Zhu, J. P. Hare, H. W. Kroto, D. R. M. Walton, K.-R. Ph, M. Ruhle, J. P. Zhang, A. K. Cheetham, Appl. Phys. Lett. 75 (1999) 3932-3934.
16. K. Chizari, A. Vena, L. Laurentius, U. Sundararaj, Carbon 68 (2014) 369-379.
17. P. Chen, L. M. Chew, A. Kostka, M. Muhler, W. Xia, Catal. Sci. Technol. 3 (2013) 1964-1971.
18. L. Roldau, S. Armenise, Y. Marco, E. Garcia-Bordejé, Phys. Chem. Chem. Phys. 14 (2012) 3568-3575.
19. S. Huang, L. Dai, A. W. H. Mau, J. of Phys. Chem. B 103 (1999) 4223-4227.
20. S. Trasobares, O. Stéphan, C. Colliex, G. Hug, W. K. Hsu, H. W. Kroto, D. R. M. Walton, Eur. Phys. J. B 22 (2001) 117-121.
21. M. Glerup, M. Castignolles, M. Holzinger, G. Hug, A. Loiseau, P. Bernier, Chem. Commun. (2003) 2542-2543.
22. G. Tuci, C. Zafferoni, A. Rossin, A. Milella, L. Luconi, M. Innocenti, L. Truong-Phuoc, C. Duong-Viet, C. Pham-Huu, G. Giambastiani, Chem. Mater. 26 (2014) 3460-3470.
23. Ziyin Lin, Gordon H. Waller, Yan Liu, Meilin Liu, Ching-ping Wong, Carbon 53 (2013) 130-136
24. R. Othman, A. L. Dicks, Z. Zhu, Inter. J. Hydro. Ener. 37 (2012) 357-372.
25. L. Qu, Y. Liu, J.-B. Baek, L. Dai, ACS Nano 4 (2010) 1321-1326.
26. K. Gong, F. Du, Z. Xia, M. Durstock, L. Dai, Science 323 (2009) 760-764.
27. C. He, Z. Li, M. Cai, M. Cai, J.-Q. Wang, Z. Tian, X. Zhang, P. K. Shen, J. Mater. Chem. A 1 (2013) 1401-1406.

28. Zhang P., Sun F., Xiang Z., Shen Z., Yun J., Cao D., Ener. Environ. Sci. 7 (2014) 442-450.

29. K. Chizari, I. Janowska, M. Houllé, I. Florea, O. Ersen, T. Romero, P. Bernhardt, M. J. Ledoux, C. Pham-Huu, Appl. Catal. A: Gen. 380 (2010) 72-80.

30. J. Chlistunoff, J. Phys. Chem. C 115 (2011) 6496-6507.

31. I. Florea, O. Ersen, R. Arenal, D. Ihiawakrim, C. Messaoudi, K. Chizari, I. Janowska, C. Pham-Huu, J. Am. Chem. Soc. 134 (2012), 9672-9680.

32. O. A. Stonkus, L. S. Kibis, O. Y. Podyacheva, E. M. Slavinskaya, V. I. Zaikovskii, A. H. Hassan, S. Hampel, A. Leonhardt; Z. R. Ismagilov, ChemCatChem 6 (2014) 2115-2128.

33. Y. T. Lee, N. S. Kim, S. Y. Bae, J. Park, S.-C. Yu, H. Ryu, H. J. Lee, J. of Phys. Chem. B 107 (2003) 12958-12963.

34. J. P. Tessonnier, D. S. Su, ChemSusChem 4 (2011), 824-847.

35. Bobby G. Sumpter; Vincent Meunier; José M. Romo-Herrera; Eduardo Cruz-Silva; David A. Cullen; Humberto Terrones; David J. Smith; Mauricio Terrones, ACS Nano. 1 (2007) 369-375.

36. J. H. Bitter, J. Mater. Chem. A 20 (2010) 7312-7321.

37. S. Biniak, G. Szymanski, J. Siedlewski, A. Wiatkoski, Carbon 35 (1997) 1799-1810.

38. H. C. Choi, J. Park, B. Kim, J. Phys. Chem. B 109 (2005) 4333-3440.

39. V. V. Strelko, N. T. Kartel, I. N. Dukhno, V. S. Kuts, R. B. Clarkson, B. M. Odintsov, Surf. Sci. 548 (2004) 281-290.

40. T. Sharifi, F. Nitze, H. R. Barzegar, C. W. Tai, M. Mazurkiewicz, A. Malolepszy, L. Stobinski, T. Wagberg, Carbon 50 (2012) 3535-3541.

41. W. Y. Wong, W. R. W. Daud, A. B. Mahamad, A. A. H. Kadhum, K. S. Loh, E. H. Majlan, K. L. Lim, Electrochimica Acta 129 (2014) 47-54.

42. U. A. Paulus, T. J. Schmidt, H. A. Gasteiger, R. J. Behm, J. Electroanal. Chem. 495 (2001) 134-145.

43. P. D. Beattie, V. I. Basura, S. Holdcroft, J. Electroanal. Chem. 468 (1999) 180-192.

44. L. Jiang, A. Hsu, D. Chu, R. Chen, J. Electrochem. Soc. 156 (2009) 370-376.

45. N. M. Markovic, P. N. Ross, Jr., Surf. Sci. Rep. 45 (2002) 117-229.